Experimental study of flame spread underneath photovoltaic (PV) modules

Experimental study of flame spread underneath photovoltaic (PV) modules

Jens Steemann Kristensen[a*], Farah Binte Mohd Faudzi[b], Grunde Jomaas[a]
[a] School of Engineering, BRE Centre for Fire Safety Engineering, University of Edinburgh, Edinburgh EH9 3JL, j.kristensen@ed.ac.uk, grunde.jomaas@ed.ac.uk
[b] International Master of Science in Fire Safety Engineering (IMSFE), Ghent University, B-9000 Ghent, Belgium
*Corresponding author

Highlights:

- 3 cm gap height reduction resulted in 6 times faster flame spread rate
- Changing the inert plate with PV modules did not increase the flame spread rate
- Increased gap height can reduce the fire risk associated with PV modules on roofs

Abstract:

The horizontal flame spread underneath a photovoltaic (PV) module (or a plate) was studied for various gap heights to understand the fundamental fire dynamics between it and a flat roof construction. In a number of experiments, an opaque black polymethyl methacrylate (PMMA) and a black stainless-steel plate were used as surrogate fuel and module, respectively. Additional experiments were conducted with actual PV modules to analyse the reproducibility of the surrogate results and to study the potential effect of the small fuel contribution from the PV modules. PMMA samples (70 cm long) of varying widths (20 cm, 30 cm and 40 cm) were ignited at one end, and flame spread rate, mass loss, radiative heat flux and temperatures were recorded. For the 30 cm wide samples, a reduction in gap height from 20 cm to 17 cm resulted in a significant increase in the flame spread rate (from 0.37 mm/s to 2.41 mm/s). A similar critical gap height (transition into a much faster flame spread rate) was identified for all widths. Thus, introducing gap height requirements into PV installation standards could offer an inexpensive and elegant design that could reduce the fire risk associated with PV modules on flat roofs significantly.

Keywords: Flame spread, heat transfer, photovoltaic (PV) installations, fire growth

1. Introduction

Photovoltaic (PV) power generation has increased by a factor of about 40 in the last decade. [1][2]. This growth is both driven by the pursuit towards fossil free energy sources and the development of economically sustainable PV systems [3][4] that can be installed in various scales; from domestic household-installations to state-owned solar farms. An increasingly common application of PV system is the utilisation of extensive flat roof construction found on warehouses.

However, the installation of a PV system on flat roof constructions introduces an increased probability of ignition [5][6][7]. In addition, it also alters the existing roof construction, and thereby the fire dynamics upon ignition. The recent dispute between Walmart and Tesla highlight the severity of the potential hazard, as Walmart have requested Tesla to remove PV installations from more the 240 of their stores, since seven of the installations had caught fire in the last 7 years [8]. Inspections of 29 PV installations, revealed 48 conditions that rendered the sites unsafe

or potentially unsafe [9], which affirmed the significant probability of ignition related to such installations.

If ignition occurs, the physical presence of the PV system changes the fire dynamics by forming a gap between the backside of the PV modules and the otherwise open roof construction [10]. This highlights the limitations in tests methods related to flame spread on roof constructions such as North American UL 790 or the European EN1187 which does not account for this change in fire dynamics. These standard test methods are designed to ensure that compliant roof covering materials are unable to facilitate the spread of fire. However, fire incidents involving PV installations on warehouse roofs resulting in considerable damage [5][11][12], such as the ASKO fire in Norway (2018, $23M loss) [13] or the Californian Walmart fires in Indio (2018, 3 injured, $1M loss) [14] and Milpitas (2016) [15] raise concerns on the validity of these tests in such scenarios. Hence, roofing materials compliant with the aforementioned standards may be undermined when the boundary conditions are modified and understanding of the altered fire dynamic scenario is of relevance. Previous studies have revealed that the deflection of the flames on the underside of the PV module from an initial fire on the roof is one of the main fire related hazards related to photovoltaic installations [10]. This is because the deflected flame cause a more rapid pre-heating of the solid ahead of the flame front, whereupon facilitating the propagation of the initial fire away from its origin to the edge of the installation [16].

Even though the mechanisms that drive flame spread are known, the majority of current research focus on large scale experiments, such as the experiments carried out by Backstrom and various co-authors for UL [17]–[25], Kristensen and Jomaas [16], or the series of large-scale experiments planned by Sipe for NFPA [26]. Through these experiments, flame spread is studied for a specific system with set characteristics, such as roofing material, geometry, mounting system and PV module. As each component introduce a myriad of unknown fire related parameters – the methods adopted in these experiments are reduced to simple pass/fail-test which cannot be substantiated with a fundamental understanding of the flame spread mechanisms. Such tests do not provide a clear understanding on how the individual components affect the fire dynamic system and thereby, unable to contribute to the overall understanding of the installation's complex fire behaviour. Furthermore, the influence of the PV modules both as a physical object and a fire load, is unknown. Therefore, it is essential to understand horizontal flame spread in gaps and quantify the effect of geometry and material properties.

Other variables to consider include the gap height and inclination angles of PV installations with respect to the roof. To optimise the energy production, PV systems are often installed at an inclined angle. On flat roof constructions, this inclination aided by the mounting system is set at an optimal angle based on the geographic location. Upon ignition, this mounting system could also contribute to increased fire load depending on material selection [16], while the geometry of the PV module can cause deflection of the flames from the initial fire [10]. As the angle of inclination varies across different installations, a fundamental analysis of flame spread below a horizontal panel is essential before introducing the influence of inclinations. This is supported by previous research which revealed that the smallest gap distance is expected to be most critical from a fire safety point of view due to increased heat flux [10], [27]. Thus, the current experiments are configured to form an understanding on how a non-combustible panel affect the initial stages of flame spread and subsequently compare these results to the influence of a PV module.

The introduction of the panel, regardless of its combustibility, generates a range of changes to the simplified heat transfer model defined by Quintiere for horizontal flame spread (Fig. 1a and Eq. (1) [28], where ρ, c_p, d and T_{ig} are the density [kg/m^3], specific heat [$J/(kg \cdot K)$], thickness [m] and ignition temperature [K] of the thin fuel, T_s and $T(x)$ are the initial temperature [K] and temperature [K] of the control volume. $\dot{q}''_f(x)$ is the heat flux [W/m^2] towards the control volume. v_p and x_p are the flame front velocity [m/s] and location [m] of the pyrolysis zone front, and σ and T_∞ are the Stefan-Boltzmann constant [$W/(m^2 \cdot K^4)$] and the ambient temperature [K].

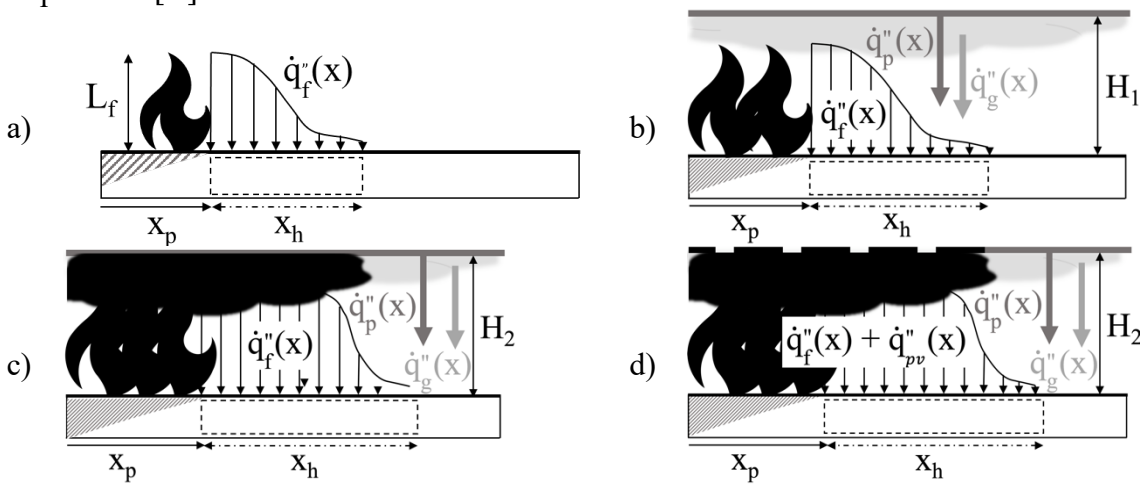

Fig. 1. Schematic of heat flux gains towards the heated control volume indicated as the pre-heating zone (x_h) in front of the pyrolysis zone (x_p), as a function of gap height (H_n), flame height (L_f) and combustible content of the panel. (a) No panel – natural flame spread, $\dot{q}''_f(x)$ - heat flux from flame. (b) Non-combustible panel, $H_1 > L_f$, heat flux from panel, $\dot{q}''_p(x)$, and accumulated smoke, $\dot{q}''_g(x)$. (c) Non-combustible panel, $H_2 < L_f$, deflection of flame causing increased heat flux from flame. (d) PV module with combustible backside membrane resulting in the heat flux $\dot{q}''_{PV}$.

These changes are caused by the heat feedback from the smoke layer, the hot panel and the deflected flame and will contribute to an increased heat flux towards the pre-heating (x_h) and pyrolysis (x_p) zones (Figs. 1a-c). Furthermore, the combustible backside of the PV module might also act as an additional fuel (Fig. 1d).

$$\rho c_p d v_p (T_{ig} - T_s) = \int_{x_p}^{\infty} [\dot{q}''_f(x) - \sigma(T^4(x) - T_\infty^4)]dx \quad (1)$$

Although quantifying the different types of heat transfer mechanisms are important for the understanding of the fire dynamics scenario, an attempt to do so will result in a heavily instrumented experimental set-up that would influence the results and analysis. Thus, the experiments herein aim to compare the heat flux required to achieve the absorbed flame spread rate, $\dot{q}'_{FSR}$, with the net radiative heat flux absorbed by the control volume, $\dot{q}'_{NET}$ - equivalent to the left and right side of Eq. (1), respectively. As one directional flame spread is assumed for the set-up, the corresponding heat flux will be represented by $\dot{q}'$. It is acknowledged that a more quantitative analysis could be of scientific interest, but the authors have decided to limit the level of fundamental understanding to a combined heat flux, $\dot{q}'$.

2. Experimental Method

Experiments were carried out both with and without PV modules. The experiments without modules were used as baseline tests to determine the steady flame spread rate (FSR), which could be used as a reference FSR for comparison with experiments with different gap heights. As the fire related properties varies for both roofing membranes (bitumen, TPO-, PVC- or EPDM-based materials) and PV modules, the experiments were carried out with generic surrogate materials to decouple the effects of the different material properties from the fire dynamics of the system. The roofing membrane was substituted with 2 mm opaque black polymethyl methacrylate (PMMA), assumed to be thermally thin, which is a well-studied reference material for flame spread rate experiments [29] [30]. Likewise, the majority of the experiments were conducted with a 3 mm thick stainless-steel plate, which was mechanically supported to prevent deflection when heated. As the PMMA was black and the stainless-steel was painted with black high absorbance and high heat resistant paint, the surfaces were assumed to be blackbodies. As the backside of a PV module consist of a combustible plastic film, five experiments were conducted with modules produced by two manufacturers. These experiments were compared to the similar experiment conducted with the stainless-steel panel. The PV modules and the stainless-steel panel had similar dimensions, i.e. a length of 1.7 m and a width of 1.0 m.

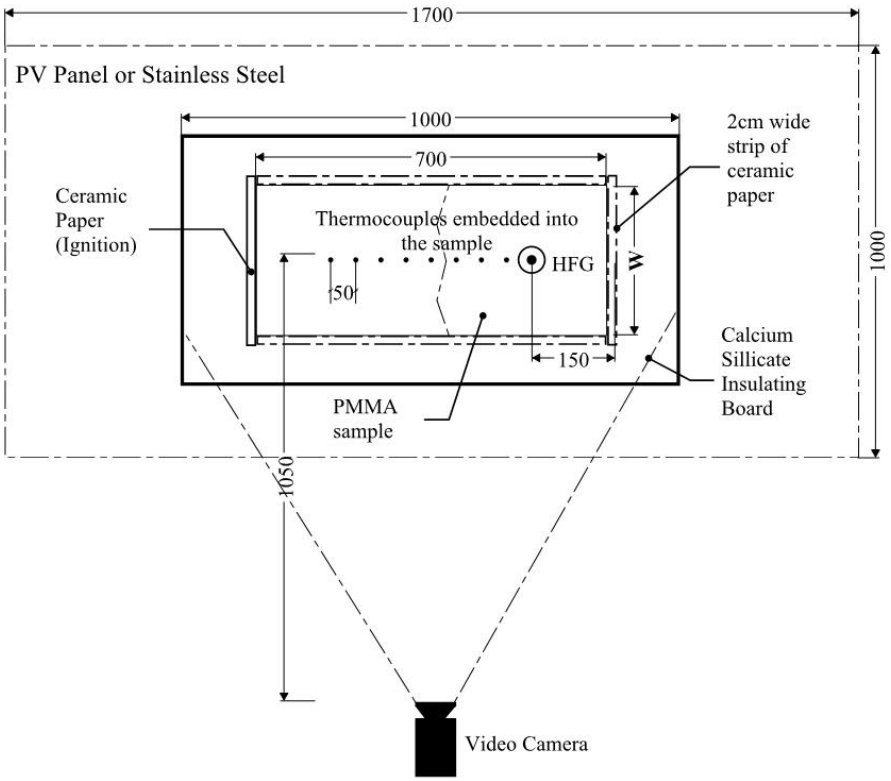

Fig. 2. Top view of the experimental set-up. All dimensions in mm.

2.1 Dimensions, installation and ignition of the PMMA samples

The PMMA was laser cut into samples of 70 cm in length of different widths (20 cm, 30 cm and 40 cm) as shown in table 1. The sample width was varied as the flame emissivity, according to Kirchhoff's law, is derived from the emission coefficient and the characteristic length of the

sample [29], [31], [32]. Hence, the radiative fraction became more dominant when the sample width was increased, which according to Jiang et al. [29], leads to an increased FSR, when they studied PMMA samples with widths between 5 and 10 cm. It is of interest to study the relation between sample width and critical gap height, as the critical height might stagnate.
The gap heights in the experimental matrix (table 1) were not based on any recommendations, as the study aims to obtain a fundamental understanding of the horizontal gap, and thus, not to give any recommendations related to actual PV installations. Understanding the influence of the gap height is crucial for understanding the complex system and cannot stand alone as a single way to obtain a safe roof construction.
The samples were installed on a 22 mm thick calcium silicate base plate with a thermal conductivity of 0.06 W/(m K) at 20°C. Eight shielded thermocouples, 14-gauge type-k, were installed through holes along the centreline of the base plate, with a distance of 5 cm between the thermocouple tips which were protruding 1 mm above the base plate. A blowtorch was used to heat the thermocouple tips before a PMMA sample was installed on the base plate. The heated thermocouple tips were imbedded in the PMMA as it cooled down. As the temperature distribution was assumed uniform through the depth of the thin fuel, the surface temperature could be determined from the thermocouple tips embedded into the fuel. As PMMA had the propensity to deflect due to localized heating, all samples were laser cut into two pieces to ensure a manageable installation process of the PMMA sample and ensure good contact between the thermocouples and the sample. A zigzag cut was used across the centre of the length to ensure proper alignment of the two sections.

Ceramic paper with a thickness of 2 mm and a width of 20 mm was placed along the edges of the sample to prevent flame spread along the edges. The paper strip at the left end of the sample (Fig. 2) was soaked in 5 g of methanol for each 10 cm of sample width. Therefore, a consistent ignition method was used and the initial flame spreads linearly along the sample.

Table 1. Number of experiments conducted for different sample widths and gap heights. Numbers in parenthesis are experiments conducted with PV modules.

		Gap height						
		12 cm	**15 cm**	**17 cm**	**20 cm**	**22 cm**	**25 cm**	**No Panel**
Sample width	**20 cm**	1	2	3	1	1	-	4
	30 cm	1	7 + (2)	6 + (1)	6 + (2)	2	-	4
	40 cm	-	-	1	1	1	1	3

2.2 Measurements

The base plate was installed on a laboratory jack, to vary the gap distance. An Ohaus laboratory scale with a precision of 0.1 g formed the base of the whole set-up. A camcorder (Panasonic HC-V770 HD, 25fps) was installed at a distance of 105 cm from the centre point of the PMMA sample. The recordings were analysed in MATLAB by monitoring the flame front location along the centreline of the sample with a binary conversion of one frame per second.
The radiative heat flux was measured by a Schmidt-Boelter heat flux gauge (Hukseflux SBG01-020), installed through a ø50 mm laser-cut hole at a distance of 550 mm from the ignition line. The heat flux gauge (HFG) was protected by a quartz disc flushed with the sample to protect the sensor from direct flame impingement and dripping. The location of the HFG enabled measurement of the radiative heat flux incident on the pre-heated zone as the flame front approaches and also the heat flux within the pyrolysis zone as the flame front travelled across it.

A quartz disc of a significant larger diameter than the heat flux gauge was used to provide sufficient buffer around the gauge as the outer ring of the quartz disc had a tendency to become translucent due to condensation of the hot pyrolysis products on the cold surface of the quartz disc. Three thermocouples, similar to ones embedded in the PMMA, were installed above the HFG to measure the gas temperature. The thermocouples were installed through a hole in the stainless-steel plate at a distance of 2 cm, 4 cm and 7 cm from the panel.

3. Results

As the ignition method for all experiments were carried out identically, the initial phases of the experiments were very similar. The left edge of the PMMA sample was heated by the burning methanol, whereupon the pyrolysis gases ignited, and a self-sustained flame front was established (Fig. 3 a). As the flame front travelled onto the virgin PMMA, the pyrolysis zone became gradually larger. For experiments above a certain critical height, a constant pyrolysis zone length and thus, a steady, constant flame spread rate was achieved.

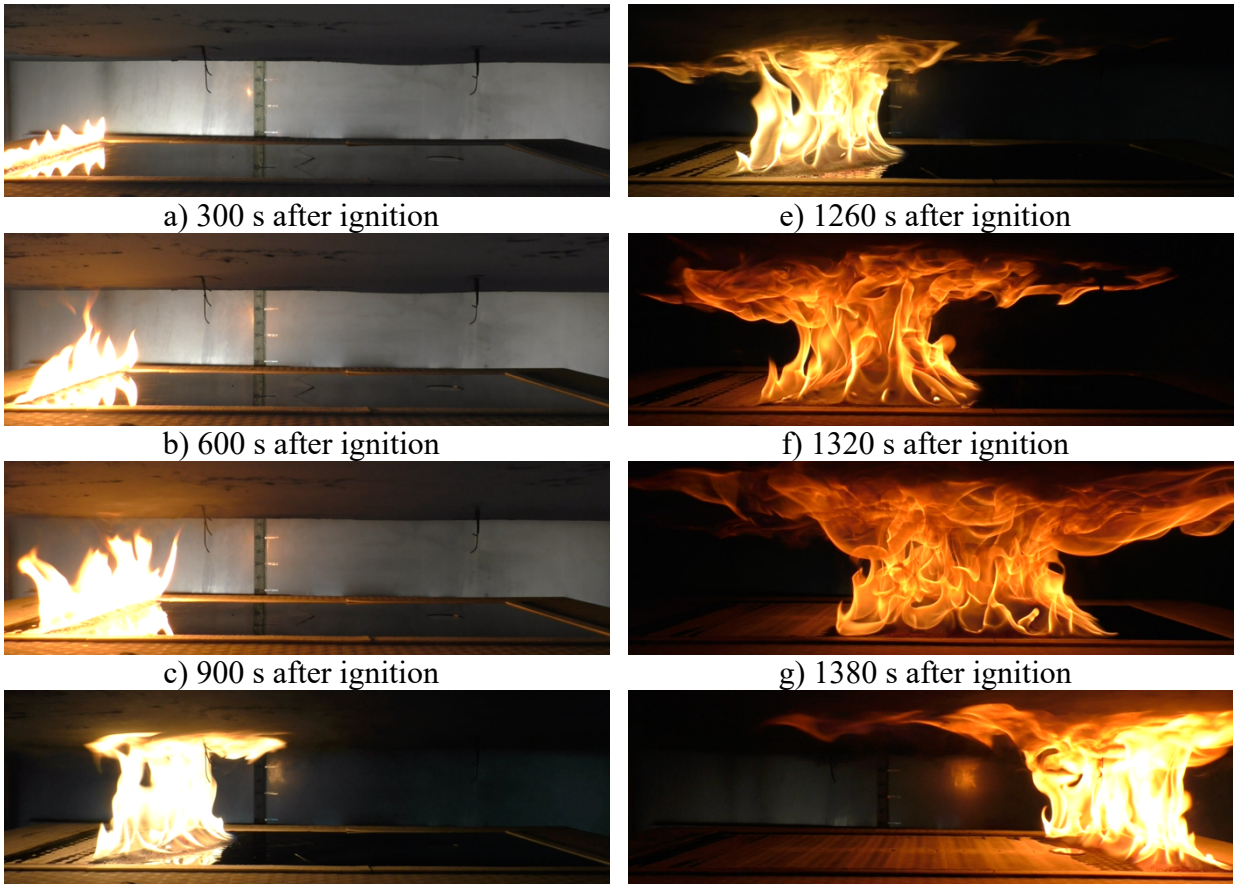

a) 300 s after ignition
e) 1260 s after ignition
b) 600 s after ignition
f) 1320 s after ignition
c) 900 s after ignition
g) 1380 s after ignition
d) 1200 s after ignition
h) 1440 s after ignition

Fig. 3. Fire development along the 70 cm PMMA plate for experiments with a gap height of 15 cm and a sample width of 30 cm. Note that the time interval changes from 300 seconds to 60 seconds after 1200 seconds.

Reduction of the gap height caused a growing heat feedback from the above horizontal panel, which gave rise to the enhanced pyrolysis-zone length and increased flame height (Fig. 3 b). This causes a loop effect of increased heat production and feedback to the pre-heating zone. When the

growing phase loop lead to a flame height which exceeded the gap height, the flame was deflected below the panel (Fig. 3 d). Thus, the heat towards the pre-heating zone grew significantly [10], whereupon the flame spread transitioned to a phase with significantly faster flame spread rate. The difference between the two phases is apparent in Fig. 3, where the approximate distance travelled by the flame front 1200 seconds after ignition (Fig. 3 d) is equal to the distance travelled from the 1260 to the 1320 second (Figs. 3 e-f).

3.1 Flame spread rate

The baseline tests (no panel) showed a clear trend, where the flame spread rates were proportional with the sample width (Fig. 4 a).

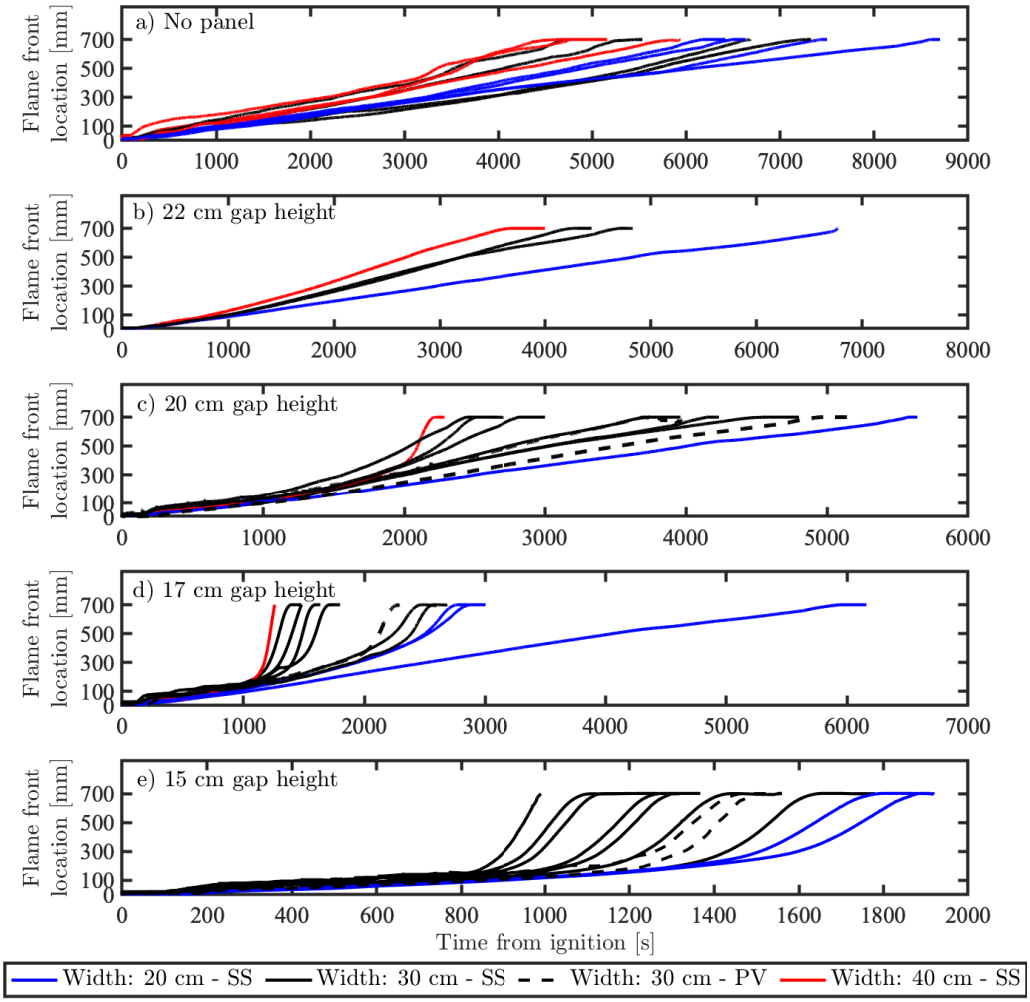

Fig. 4. Location of flame front as a function of time from ignition at various gap heights.

For all experiments, the flame spread rates were similar along the first 10 cm of the PMMA sample. Whereas the visual difference between the three sample widths for the baseline experiments was limited, the presence of the stainless-steel panel (Fig. 4 b) demonstrated a significant difference. The increased pre-heating zone for larger widths resulted in an enhanced heat feedback and, thus, flame spread rate. Although the flames spread rate remained constant when the stainless-steel panel was introduced above the PMMA, the overall flame spread rate was increased.

The critical gap height was defined for the cases where the presence of the panel causes a significant change in the flame spread rate during the experiments. Such a change of the flame spread rate was very apparent for the 40 cm sample when the gap height was reduced to 20 cm (Fig. 4 c). The constant flame spread rate during the initial 1000 s of the experiment was succeeded by a gradual increase as the heat feedback loop was slowly enhanced. Approximately 2000 s after ignition, a sudden increase of the flame spread rate occurred as the flame height exceeded the gap height and deflected below the non-combustible panel. Similarly, the dramatic transition occurred for the 30 cm sample when the gap height was reduced to 17 cm, where the final flame spread rate for all experiments are significantly faster than any of the experiments conducted with a gap distance of 20 cm or higher.

In general, the experiments had a good reproducibility. However, the varying onset of the fast flame spread does highlight that factors such as localized flows and minor inclinations of the PMMA could lead to minor variations in the results. Still, these minor uncertainties did not influence the qualitative results or the conclusions.

The results of the experiments conducted with PV modules (Figs. 4 d-e) did not exhibit considerable differences from the experiments with the stainless-steel plate. However, it was observed that burning droplets of molten plastic dripped from the backside of one PV module model (Fig. 5) though it did not affect the overall flame spread rate. This caused localised heating and ignited plastic materials next to the experimental setup which could increase the area of the fire in a larger domain such as that found on warehouses.

Fig. 5. Experiment conducted with PV module at a gap height of 17 cm. Flame front moving from left to right. The highlighted flames were molten plastic that continued to burn after dripping from the backside of the PV module.

3.2 Mass loss rate

In support of the flame spread results, the normalised mass loss rate (MLR) also indicated a steady flame spread rate for the baseline experiments (Fig. 6 a). The average mass loss rate, calculated according to BS ISO 5660-1 [33], was normalised with respect to the sample width facilitating comparison across widths. Subsequently, the average, normalised MLR was calculated across similar baseline experiments to compare the normalised MLR as a function of the flame fronts location.

For the baseline experiments in general, the widest sample width corresponds to the highest normalised MLR. Whereas the normalised MLR for the first 100 mm of all experiments might be affected by pre-heating from the ignition source, the following part of the plots are made up by a normalised MLR increase, possibly followed by a stable level, and a reduction around 550 mm. The stable normalised MLR observed for the baseline tests with a sample width of 20 cm (Fig. 6

a), indicate an equilibrium of the heat feedback loop, and the reduction of the normalised MLR is caused by the presence of the heat flux gauge in the centre of the sample. For the baseline tests, a stable normalised MLR is only achieved by the sample width of 20 cm, as the enhancement of the heat feedback loop is so sparse, that the stable levels for the sample widths of 30 cm and 40 cm are reached before the flame front reach the end of the sample. The introduction of the inert panel give rise to a more powerful heat feedback loop, which is further enhanced with reduction of the gap height. Thus, a faster increase of the normalised MLR (Fig. 6 b).

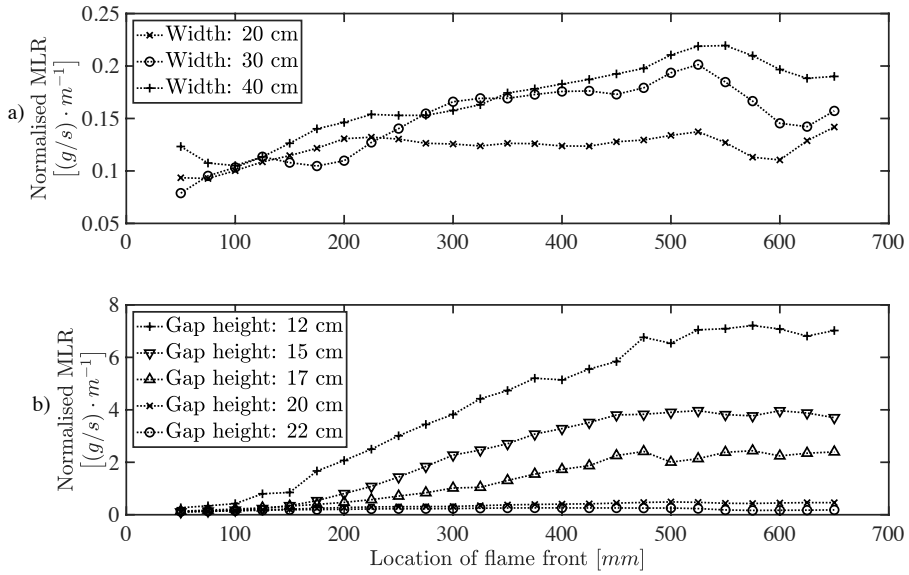

Fig. 6. Average mass loss rate normalised with respect to sample width, as a function of flame front location. a) Baseline experiments with different sample widths. b) Sample width of 30 cm with panel of stainless-steel and various gap heights.

3.3 Analysis and discussion

To quantify the effect of the above horizontal panel, the average flame spread rate (FSR) for each five centimetres were compared to the average flame spread rate for the corresponding baseline experiments. As the overall flame spread rates were constant in the baseline experiments (Fig. 4 a), an average FSR for the centre 60 cm were calculated (FSR avg. in Table 2) and used for the comparison to avoid fluctuations caused by localised changes of the baseline FSR.

For all other experiments, the FSR were calculated for each 5 cm as the average speed of the flame front between two points 10 cm apart. The method resulted in an overview of the FSR trends, rather than a FSR with local fluctuations. As such, the average flame spread rate across similar experiments could be compared to the FSR for the baseline experiments in Fig. 7.

The comparison of the relative flame spread rates (Fig. 7) demonstrates the significant effect of a gap height reduction of a few centimetres, which is particularly apparent when the gap is reduced from 20 cm to 17 cm for the sample width of 30 cm (Fig. 7 b). For the experiments where there is a transition from a slow to a faster flame spread rate, the reduction of the gap height causes two significant changes. i) a reduced time, thus distance, to the onset towards the fast flame spread, and ii) a faster increase of the relative flame spread rate. Both changes are caused by an

enhanced heat loop, which induce an increased heat feedback and thus, a longer pyrolysis zone and heat release rate.

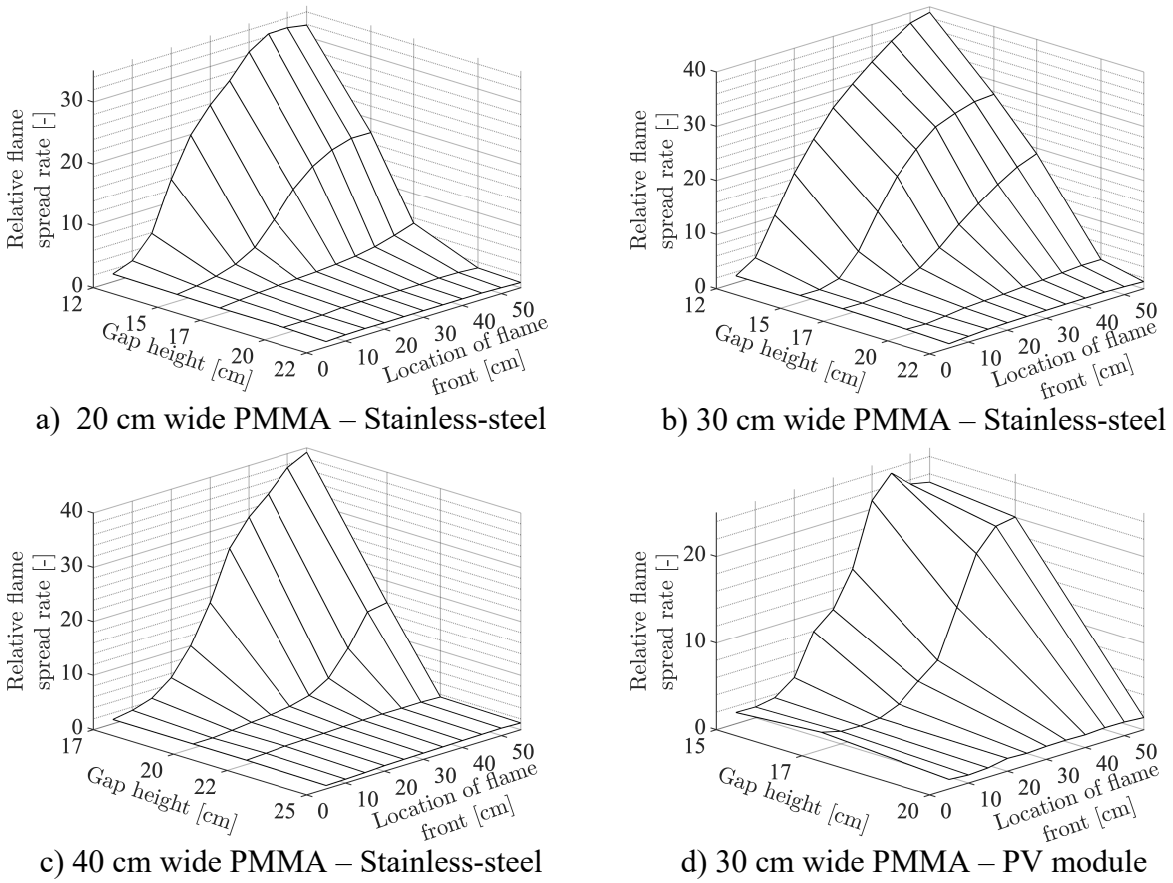

Fig. 7. Relative flame spread rate compared to the baseline flame spread rate (Table 2), as a function of gap heights and location of the flame front. Note that the ranges in the y- and z-axis vary from plot to plot.

The relative flame spread rate for the experiments conducted with PV modules (Fig. 7 d) are consistently somewhat lower than in similar experiments conducted with the inert stainless-steel panel (Fig. 7 b). This can be explained by the fact that the thermal inertia of the PV module (glass, plastic, metal) is assumed to be lower than that of stainless-steel. Thus, both the heating rate of the plate and heat loss to the surroundings will be larger for the stainless-steel plate than for the PV module. Furthermore, the absorbance and emissivity of the black surface stainless-steel plate are higher than the corresponding values of the white plastic membrane on the backside of the PV modules. Hence, the thermal properties of the stainless-steel plate might result in an enhanced heat feedback loop, which can explain the slightly lower flame spread rate in the experiments conducted with the PV modules. However, it is important to emphasize that this substitution only leads to small quantitative differences and no qualitative differences. As such, there is a critical gap height also for PV modules, though slightly different from the case-specific values reported herein.

For the experiments conducted with a gap height of 15 cm to the PV module, a slight reduction corresponding to 0.24 mm/s is noticed after the flame front has reached 45 cm. The reduction is expected to be within experimental errors.

Contrary to commercially available roofing membranes, the burning PMMA samples produced a self-sustained fire, which permits a slow growth phase over a relatively long distance before switching to the faster and more severe flame spread rate. This is not the case for commercially available roofing membranes, where the presence of flame retarders will make this process irrelevant, as the flame will be quenched if the initial growth is too slow. It is therefore more likely, that similar experiments conducted with roofing membranes will result in either immediately rapid flame spread, or no flame spread at all. In such case, a critical gap height will be more evident and, to a greater extent, rely on the initial fire size. For this reason, it would be of interest to understand the extent of the potential ignition sources to define of the range of initial fire sizes the roof construction and PV system would be designed to withstand.

For all experiments, the heat flux in the pre-heating zone (x_h), $\dot{q}'_{NET}$, was calculated at the location of the heat flux gauge according to the right side of Eqn. (1). As the location of the flame front is known as a function of time, the temperature of the PMMA and heat flux can be determined as a function of distance to the flame front, and this has been visualised in Fig. 8. The corresponding calculation of the left side of Eqn. (1) is conducted with a PMMA density, specific heat and ignition temperature of $\rho = 1.19\ g/cm^3$, $c_p = 1420\ J/(kg\ K)$ and $T_{ig} = 278\ °C$, as well as an ambient and initial PMMA temperature of $T_\infty = T_s = 25\ °C$.

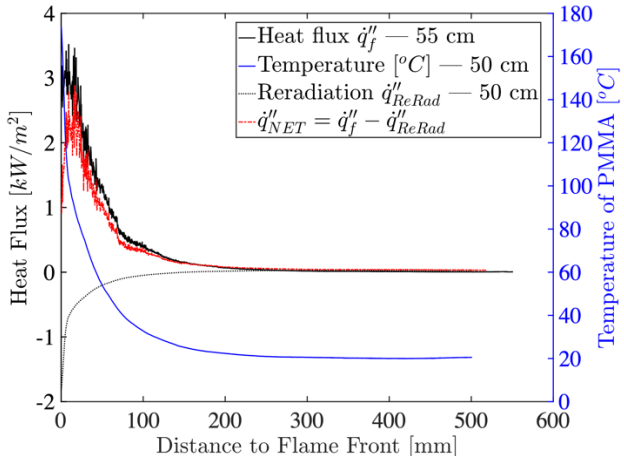

Fig. 8 Measured heat flux and temperature plotted together with the corresponding reradiation and gained heat flux at the location of the heat flux gauge. From baseline experiment with a sample width of 30 cm.

The result of the baseline tests (Table 2), indicate a correlation between the horizontal FSR and the heat flux absorbed when the flame front approaches. Consistent with the study by Jian et al. [29], the flame spread rate, hence $\dot{q}'_{FSR}$, is proportional to the sample width, which also corresponds to the raw data in Fig. 4. A similar trend is evident for the gained heat flux at the location of the heat flux gauge, $\dot{q}'_{NET}$, and there is no significant difference between the two heat fluxes for the sample width of 30 cm and 40 cm. For the baseline tests with a sample width of 20

cm, the deviation might be a consequence of the general low heat flux from the flame being outside the calibration range of used the heat flux gauge.
For the baseline tests with a sample width of 20 cm, the deviation might be a consequence of the general low heat flux from the flame being outside the calibration range of used the heat flux gauge. As the overall error across the three sample widths is limited, the assumed relation between the simplified model and experimental set-up is still fair. On this basis, it is confirmed that the instrumentation is sufficient for determining the variables in the simple heat transfer model introduced in Eq. (1).

Table 2. Average flame spread rate (FSR avg.), heat fluxes based on respectively the left, $\dot{q}'_{FSR}$, and right, $\dot{q}'_{NET}$, side of Eq. (1), and the ratio between them.

	Sample width		
	20 cm	**30 cm**	**40 cm**
FSR avg. [mm/s]	0.102	0.127	0.152
$\dot{q}'_{FSR}$ **[W/m]**	87	107	130
$\dot{q}'_{NET}$ **[W/m]**	71	117	122
$\dot{q}'_{FSR}/\dot{q}'_{NET}$ **[−]**	1.23	0.92	1.07

The proportionality between $\dot{q}'_{FSR}$ and $\dot{q}'_{NET}$ is repeated, when the panel is installed above the PMMA (Figs. 4 a-b), but the difference between the two heat fluxes reveal a trend, where $\dot{q}'_{FSR}$ becomes relatively larger than $\dot{q}'_{NET}$ when the gap distance is reduced (Fig. 4 c). The opposite trend is noticed, when the gap height is larger than the critical gap height. As the heat transfer model only account for the net radiative heat transfer, the trend could be caused by either convective heat transfer or reduced transparency of the quartz disc.

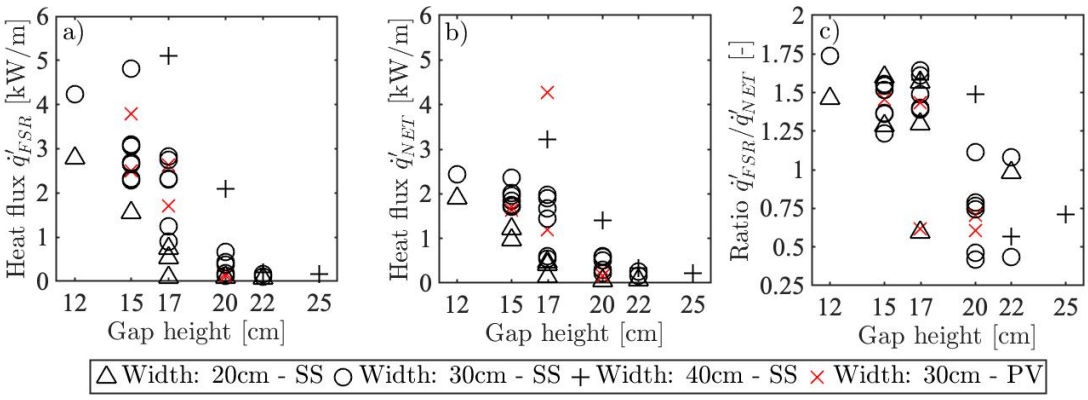

Fig. 9. Plot of heat flux at the location of the heat flux gauge. a) heat flux based on FSR, b) heat flux based on measured heat flux and reradiation, and c) ratio between the two methods.

Contrary to what is the case in the baseline experiments (no panel), the stainless-steel plate, or the PV module, obstructs the forced air flow produced by the extraction hood. When the gap distance is high and the total heat release rate is low, the forced air flow might cause an increased convective heat loss from the pre-heating zone – reducing the influence from radiative heat. However, this effect is suppressed when the gap height is reduced, whereas the combined measured heat flux, $\dot{q}'_{NET}$, is smaller than $\dot{q}'_{FSR}$. Although the gap temperature does increase as the fire changes from the growing to the accelerating phase, the raw data in Fig. 9 reveal that the rapid gas temperature increase 8 cm above the heat flux gauge corresponds well with the arrival

of the flame front. Consequently, the convective heat transfer towards the pre-heating zone ahead of the flame front is limited and it is expected that a temporary reduced transmissivity of the quartz disc causes the increased ratio between $\dot{q}'_{NET}$ and $\dot{q}'_{FSR}$. As the measured heat flux increase gradually when the quartz disc is engulfed in flames, the debris is burned away.

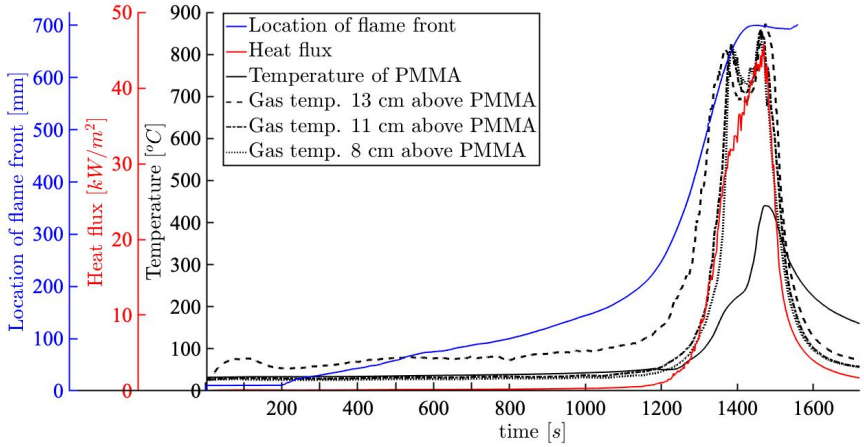

Fig. 10. Sample width: 30 cm. Gap height: 15 cm. Plot of flame front location, heat flux, temperature 5 cm in front of the HFG, and gap temperature at three heights above the HFG. Notice, that the arrival of the flame front at 700 mm is not the end of the experiment, as seen in the visual overview of the same experiment (Fig. 3 f-h)

4. Conclusions

Based on the experiments where flame spread in horizontal gaps of various heights was studied, there is a critical gap distance for which the constant low flame spread rate exhibited at gap heights above this critical value accelerates to a rapid flame spread rate for gap heights below this critical value. This occurs for gap heights below the critical value as the initial flame height at the start of ignition steadily grows until it exceeds the gap height. The flame is then deflected below the panel, which cause a significant increase of the combined heat flux towards the pre-heating zone. Thus, a rapid acceleration of the flame front occurs with up to 48 times faster flame spread rate compared to the baseline experiments. The transition from a low constant flame spread rate to an accelerated rapid flame spread rate occurs with a minute difference in gap heights (2-3 cm) which highlights the importance of gap heights in PV installations. The width of the sample, which determines the size of the initial fire did affect the critical gap height, as the critical gap height reduced when the sample width increased. Therefore, understanding of the system, with its potential source of ignition and resultant fire size, would be relevant for future studies.

The baseline experiments were found to be consistent with a simple heat transfer model based on radiative heat transfer, which are dominant in flame spread on horizontal thin fuels. However, for low gap heights between the non-combustible panel and the PMMA, the total heat flux towards the control volume was consistently lower than the heat flux required to maintain the measured flame spread rate. The difference could be caused by: i) a reduced transparency of the quartz disc protecting the heat flux gauge caused by condensation. ii) non-measurable increased convective heat flux, as the small gap distance resembles an enclosure, or iii) a combination of i) and ii). Future studies should aim to prevent conductive heat transfer from the heat flux gauge to the quartz disc, which would reduce the consequence of i).

The experiments showed no enhanced flame spread caused by the combustible components of the PV modules when compared to similar experiments conducted with a surrogate non-combustible black stainless-steel plate. These findings correspond to earlier results with used and new PV modules [10], where it was reported that the increase in measured heat fluxes was due to the re-radiation from the PV module, rather than the slightly higher fuel load associated with new modules versus burned/used panels.

The presence of a critical gap height above which flame spread damage could be minimised provides an opportunity for it to be used as an effective mitigation measure. This could be an attractive solution if the PV installation is retrofitted on an existing roof construction where the insulation materials are unknown and costly to be refurbished by which a roof fire entails a significant risk. Although this has to be co-ordinated with other design considerations such as wind loads that seek to decrease the gap heights, optimising PV installation design with a consideration of critical gap height for fire spread could lead to a more holistic design.

It is to be noted that the critical gap heights reported herein are case specific and should therefore not be used directly for recommendations in installation standards.

5. Acknowledgements

The authors would like to thank IKEA Services AB, ROCKWOOL International A/S and Kingspan Holdings (Irl) Limited for the financial support of the PhD project of Jens Steemann Kristensen. In addition, a special thanks goes to the department of Civil Engineering at the Technical University of Denmark (DTU) for hosting Jens Steemann Kristensen as a guest researcher and Farah Binte Mohd Faudzi as a guest student. The use of the DTU fire laboratory, as well as the general hospitality at DTU was highly appreciated.

6. References

[1] S. Novak, *Trends in Photovoltaic Applications: Survey Report of Selected IEA Countries between 1992 and 2009*, *IEA-PVPS*, 2010.

[2] G. Masson, I. Kaizuka, A. Detollenaere, and J. Lindahl, *2019 Snapshot of Global PV Markets*, IEA-PVPS, 2019.

[3] N. M. Haegel et al., *Terawatt-scale photovoltaics: Trajectories and challenges*, *Science*, 2017, DOI: 10.1126/science.aal1288

[4] G. Masson and I. Kaizuka, *Trends in photovoltaic applications 2018*, IEA-PVPS, 2018.

[5] A. Sepanski et al., *Assessing Fire Risks in Photovoltaic Systems and Developing Safety Concepts for Risk Minimization*, 2015 (translated to english in 2018).

[6] B. Brooks, *The ground-fault protection blind spot: A safety concern for larger photovoltaic systems in the United States*, *Sol. Am. Board Codes Stand.*, http://www.solarabcs.org/about/publications/reports/blindspot/, (accessed 04.09.19), 2012.

[7] Y. Zhao, J. de Palma, J. Mosesian, R. Lyons, and B. Lehman, *Line-Line Fault Analysis and Protection Challenges in Solar Photovoltaic Arrays*, *Ind. Electron. IEEE Trans.*, vol. 60, no. 9, 3784–3795, 2013, DOI: 10.1109/TIE.2012.2205355

[8] N. Groom and N. Balu, *Walmart sues Tesla for negligence after repeated solar system fires*, Reuters, https://reut.rs/2ZhAvgh, (accessed 08.01.20), 2019.

[9] A. Bera and A. Sarkar, *Factbox : Walmart and Tesla fought in private long before solar lawsuit*, Reuters , https://reut.rs/2Z88yMQ, (accessed 08.01.20), 2019.

[10] J. S. Kristensen, B. Merci, and G. Jomaas, *Fire-induced reradiation underneath photovoltaic arrays on flat roofs*, *Fire Mater.*, vol. 42, no. 3, pp. 316–323, 2018, DOI:

10.1002/fam.2494
[11] L. Fiorentini, L. Marmo, E. Danzi, and V. Puccia, *Fire in photovoltaic systems: Lessons learned inItaly*, *SFPE Emerg. Trends enewsletter Issue 99*, http://www.sfpe.org/?page=FPE_ET_Issue_99, (accessed 04.09.19), 2015
[12] C. C. Grant, *Fire Fighter Safety and Emergency Response for Solar Power Systems*, The Fire Protection Research Foundation, https://portal.ct.gov/-/media/CFPC/_old_files/ReportFFTacticsSolarPower51210pdf.pdf?la=en, (accessed 04.09.19), 2010.
[13] R. Stølen, R. F. Mikalsen, and J. P. Stensaas, *Solcelleteknologi og brannsikkerhet,* RISE-rapport 2018:31, Research Institutes of Sweden, https://risefr.com/media/publikasjoner/upload/2018/solceller-og-brann-rise-rapport-2018-31.pdf, (accessed 04.09.19), 2018.
[14] NBC Palm Springs, *Second-Alarm Fire at Indio Walmart Injures Three , Store Evacuated*, National Broadcasting Company, NBC Palm Springs, https://nbcpalmsprings.com/2018/05/29/firefighters-battle-two-alarm-fire-at-indio-walmart/, (accessed 04.09.19), 2018.
[15] M. Favro, *Firefighters Battle Two-Alarm Blaze at Walmart in Milpitas,* NBC Bay Area, https://www.nbcbayarea.com/news/local/Firefighters-Battle-Two-Alarm-Blaze-at-Walmart-in-Milpitas-372763132.html, (accessed 04.09.19), 2016.
[16] J. S. Kristensen and G. Jomaas, *Experimental Study of the Fire Behaviour on Flat Roof Constructions with Multiple Photovoltaic (PV) Panels*, *Fire Technol.*, vol. 54, no. 6, pp. 1807–1828, 2018, DOI: 10.1007/s10694-018-0772-5
[17] B. Backstrom and M. Tabaddor, *Effect of Rack Mounted Photovoltaic Modules on the Fire Classification Rating of Roofing Assemblies*, 2010.
[18] B. Backstrom and M. Tabaddor, *Effect of Rack Mounted Photovoltaic Modules on the Flammability of Roofing Assemblies – Demonstration of Mitigation Concepts*, 2010.
[19] B. Backstrom and D. Sloan, *Characterization of Photovoltaic Materials – Critical Flux for Ignition / Propagation Phase 3*, Northbrook, IL, USA, 2012.
[20] B. Backstrom and D. Sloan, *Validation of 42" PV Module Setback on Low Slope Roof Experiments Project 7*, 2012.
[21] B. Backstrom and D. Sloan, *Considerations of Module Position on Roof Deck During Spread of Flame Tests Phase 5*, 2012.
[22] B. Backstrom and D. Sloan, *Effect of Rack Mounted Photovoltaic Modules on the Fire Classification Rating of Roofing Assemblies Phase 2,* 2012.
[23] B. Backstrom and D. Dini, *Firefighter safety and photovoltaic installations research project*, *Proc. SPIE - Int. Soc. Opt. Eng.*, vol. 8472, 2012.
[24] B. Backstrom and D. Sloan, *Report of Experiments of Minimum Gap and Flashing for Rack Mounted Photovoltaic Modules Phase 4*, 2012.
[25] B. Backstrom, *Validation of Roof Configuration 2 Experiments Project 9*, 2013.
[26] J. Sipe, *Development of Fire Mitigation Solutions for Photovoltaic (PV) Systems Installed on Building Roofs – Ph . 1*, Fire Protection Research Foundation, https://www.nfpa.org/-/media/Files/News-and-Research/Fire-statistics-and-reports/Electrical/RFDevelopmentFireMitigationSolutions.ashx?la=en, (accessed 04.09.19), 2016.
[27] X. Ju, X. Ren, and X. Zhou, *Impact of flat roof – integrated solar photovoltaic installation mode on building fire safety*, Fire Mater. 2018, pp. 1–13, 2019, DOI: 10.1002/fam.2755

[28] J. G. Quintiere, *Fundamentals of Fire Phenomena*, John Wiley & Sons, 2006.
[29] L. Jiang, C. H. Miller, M. J. Gollner, and J. H. Sun, *Sample width and thickness effects on horizontal flame spread over a thin PMMA surface*, *Proc. Combust. Inst.*, vol. 36, no. 2, pp. 2987–2994, 2017, DOI: 10.1016/j.proci.2016.06.157
[30] A. C. Fernandez-pello and T. Hirano, *Controlling Mechanisms of Flame Spread*, *Fire Sci. Technol.*, vol. 1, pp. 17–54, 1982, DOI: 10.1080/00102208308923650
[31] D. Drysdale, *Ignition: The Initiation of Flaming Combustion*, in *An Introd. to Fire Dyn.*, John Wiley & Sons, 2011, pp. 225–275.
[32] J. de Ris, Fire radiation—a review, *Symp. Combust.*, 1979, DOI: 10.1016/S0082-0784(79)80097-1
[33] British Standard ISO, *BS ISO: 5660-1:2015 Reaction-to-fire tests — Heat release, smoke production and mass loss rate, Part 1: Heat release rate (cone calorimeter method),* 2015.

Figure captions

Table captions